FRONT PROPAGATION OF ICE SLURRY STRATIFICATION PROCESSES

P.W. EGOLF, D. VUARNOZ, O. SARI, D. ATA-CAESAR, A. KITANOVSKI[1]

University of Applied Sciences of Western Switzerland
Institute Génie Thermique
CH-1401 Yverdon-les-Bains, Switzerland
Peter.egolf@eivd.ch

The combined stratification and melting of ice particles of ice slurries is theoretically described by multi-component fluid dynamics and the Continuous-Properties Model (CPM) for melting and freezing, applied only to melting. Ice particle stratifications with isothermal conditions are studied. Particle distributions as a function of height in the storage tank and time are presented. Calculated front propagation times are compared with experimental results; they compare well. Furthermore, they show that ice particles with an approximate diameter of 200 μm, in the average, yield clusters with an equivalent diameter of 500 μm.

1. INTRODUCTION

Only few investigations of ice particle fields in storage tanks exist. Storage of ice slurries for air-conditioning applications with low ice fractions have been performed by Kozawa et al. (see [1] and [2]). Hong, Kawaji, and Goldstein performed numerical investigations of flow fields in a storage tank with forced advection generated by a propeller mixing device by applying the commercially available Fluent simulation code [3]. Meili et al. showed that - after turning off the mixer - homogeneous temperature and also ice particle fields are obtained again, if the mixer is taken into operation after a twelve hours intermission [4]. These conclusions were mainly based on temperature measurements and taking only few ice slurry samples from the tank. Vuarnoz et al. determined stratification processes with initial homogeneous ice particle fields of 10.3 % and 21.4 % ice fraction by sucking samples from four different levels in a tank and investigating them under a light-transmittance microscope [5]. Egolf et al. performed first academic examples of numerical calculations of isothermal stratification processes with an ideal maximal packing factor of hundred percent [6] and a more realistic upper bound of seventy four percent [7]. This article is a continuation of the work presented in Ref's [5],[6] and [7].

2. THEORY OF ISOTHERMAL STRATIFICATION

Here the theory describing non-isothermal stratification is only summarized, because a detailed derivation, starting with the ice particle density *n*, is presented in [6]

[1] During PhD work on visit for one month in Yverdon-les-Bains. Home address: Prof. A. Poredos, University of Ljubljana, Faculty of Mechanical Engineering, Ljubljana, Slovenia.

$$\frac{\partial \hat{\rho}_I}{\partial t} + div\left(\hat{\rho}_I \vec{v}_I\right) - D\rho\Delta c_I - \rho\rho_I V_p q_p = 0. \tag{1}$$

The weighted density of the ice (particle) component is

$$\hat{\rho}_I = \rho\ c_I, \tag{2}$$

in agreement with the theory of multi-component fluid dynamics. The first term describes instationarity of the ice component, the second is the convective term, the third the diffusion term, and the fourth the sink/source term. The last term is important, if melting is taken into consideration. In chapter 7 a flux density is introduced, which is defined by

$$\vec{j} = \hat{\rho}_I \vec{v}_I. \tag{3}$$

3. THEORY OF NON-ISOTHERMAL STRATIFICATION

In Ref. [7] the theory for stratification and melting has been presented. Important is the last term of equation (1), which couples the thermodynamic behaviour of the ice particles with their fluiddynamic features. It follows

$$W = \rho_I V_p \ell, \tag{4}$$

where ℓ denotes the latent heat of the water-ice phase transition.

The number of particles destroyed by melting multiplied by the work to destroy one particle is identical to the heating power per unit of mass

$$q_p\ W = \frac{1}{\rho} div\ \dot{q}. \tag{5}$$

From this equation, and also by substituting the right-hand side of equation (4), it follows that

$$\rho_I V_p q_p = \frac{1}{\rho\ \ell} div\ \dot{q}. \tag{6}$$

This is introduced into (1). After introducing Fouriers law and applying some basic calculations (see Ref. [7]) one obtains

$$\frac{\partial \hat{\rho}_I}{\partial t} + div\left(\rho_I \vec{v}_I\right) - D\rho\Delta c_I + \frac{1}{\ell}\left[\frac{dk}{dT}(\nabla T)^2 + \frac{dk}{dc_I}\left(\nabla c_I \nabla T\right) + k\Delta T\right] = 0. \tag{7}$$

In the case of melting this equation must be combined with a melting model. We apply the Continuous-Properties Model (CPM), which is generally introduced in Ref. [8] and applied

for the first time to ice slurries in Ref. [9]. If stratification occurs, the ice fraction is independent of the temperature. Then the CPM must be slightly generalized to become

$$\frac{\partial T}{\partial t} - \alpha \left\{ \frac{1}{k} \left[\frac{dk}{dT} (\nabla T)^2 + \frac{dk}{dc_I} \left(\nabla c_I \nabla T \right) \right] + \Delta T \right\} = 0, \qquad \alpha = \frac{k}{\rho \, c_p} . \tag{8a,b}$$

The two initial conditions are defined by a homogeneous temperature and ice particle distribution in the fluid domain Γ

$$\chi(t=0,\vec{x}) = \chi_0 = c, \quad \forall \vec{x} \in \Gamma, \quad \chi \in \{T, c_I\}. \tag{9}$$

The boundary condition for the particle flux is

$$\left[\hat{\rho}_I \vec{v}_I (t,\vec{x}) - D \nabla \hat{\rho}_I (t,\vec{x}) \right] \vec{\gamma} = 0. \tag{10}$$

The second boundary condition describes the heat flux density, which is caused by a temperature difference between the ice slurry temperature T at the inside of the wall of the tank and the ambient temperature T_A of the storage tank

$$\left[T_A - T(t,\vec{x}) \right] = -\frac{k}{U} \left[\nabla T(t,\vec{x}) \vec{\gamma} \right], \forall \vec{x}, \vec{\gamma} \in \partial\Gamma . \tag{11}$$

4. EXPERIMENTAL INVESTIGATIONS OF ICE PARTICLE SHAPES

The experimental method, the test facility and the evaluation techniques have already been presented in Ref. [5]. In the first steps, leading to the results in the previous article, statistical evaluations of characteristic ice particle sizes were only performed for the initial time (t=0), when stratification just starts to occur. At later times only the number of ice particles were counted and the evaluation was performed with the statistical material, e.g. effective mean length and effective mean width, obtained at t=0. On the other hand slight alterations of ice particle shapes as a function of time are observed. A varying velocity with changing diameter leads to an alteration of the statistical properties as a function of time. In stratification processes particles of larger diameters show smaller settling times and vice versa. In Table 1 and FIG. 1 statistical informations on ice particle shapes and sizes are presented as a function of time and space. The evaluations to determine the space dependence were performed by removing samples at different heights, namely at four levels at which ice slurry probes can be taken from the storage tank. The additional information led to the possibility of improving some earlier published results.

It can be seen that the ice particles become smaller as a function of time. This is in contradiction to the observations of a time-dependent increase of particle size (time behaviour). But

Approximate time Position	0’	3.5’	11’	13’
Level 1	N / Ne= 846.5 / 50 c_I=38.5 % $\langle l_{eff} \rangle$= 280.6 µm $\langle b_{eff} \rangle$= 188.3 µm σ l_{eff} =9.6 µm σ b_{eff}= 48.2 µm <t> = 0 ’’	N / Ne= 560.1 / 50 c_I= 27.1 % $\langle l_{eff} \rangle$= 285.7 µm $\langle b_{eff} \rangle$= 185.0 µm σ l_{eff} = 101.6 µm σ b_{eff}= 59.9 µm <t> = 2’30’’	N / Ne= 569.2 / 50 c_I= 18.9 % $\langle l_{eff} \rangle$= 259.6 µm $\langle b_{eff} \rangle$= 165.7 µm σ l_{eff} = 74.3 µm σ b_{eff}= 49.1 µm <t> = 10’15’’	N / Ne =674.9 / 50 c_I= 23.7 % $\langle l_{eff} \rangle$= 256.1 µm $\langle b_{eff} \rangle$= 163.85 µm σ l_{eff} = 112.3 µm σ b_{eff}= 50.9 µm <t >= 14’00’’
Level 2	N / Ne= 637.1 / 50 c_I= 27.4 % $\langle l_{eff} \rangle$= 274.9 µm $\langle b_{eff} \rangle$= 185.7 µm σ l_{eff}= 89.2 µm σ b_{eff}= 49.00 µm <t> = 0 ’’	N / Ne= 579.6 / 50 c_I= 26.7 $\langle l_{eff} \rangle$= 269.8 µm $\langle b_{eff} \rangle$= 184.1 µm σ l_{eff}= 97.6 µm σ b_{eff}= 61.2 µm <t >= 3’0’’	N / Ne = 28.6 / 25 c_I =0.5 % $\langle l_{eff} \rangle$= 215.0 µm $\langle b_{eff} \rangle$= 133.1 µm σ l_{eff}= 73.1 µm σ b_{eff}= 48.7 µm <t> = 10’00’’	N / Ne = 18.3 / 15 c_I= 0.04 % $\langle l_{eff} \rangle$= 219.0 µm $\langle b_{eff} \rangle$= 143.2 µm σ l_{eff}= 87.8 µm σ b_{eff}= 48.8 µm <t >= 12’45’’
Level 3	N / Ne= 895 / 50 c_I = 32.6 % $\langle l_{eff} \rangle$= 256.4 µm $\langle b_{eff} \rangle$= 171.6 µm σ l_{eff}= 92.2 µm σ b_{eff}= 53.7 µm <t>= 0 ’’	N / Ne= 237.3 / 50 c_I = 6.6 % $\langle l_{eff} \rangle$= 240.6 µm $\langle b_{eff} \rangle$= 155.9 µm σ l_{eff}= 79.3 µm σ b_{eff}= 50.4 µm <t>=3’30’’	N / Ne = 26 / 20 c_I = 0.5 % $\langle l_{eff} \rangle$= 193.7 µm $\langle b_{eff} \rangle$= 144.3 µm σ l_{eff}= 80.9 µm σ b_{eff}= 54.5 µm <t >= 11’22’’	N / Ne =24 c_I = 0.3 % $\langle l_{eff} \rangle$= 187.4 µm $\langle b_{eff} \rangle$= 124.6 µm σ l_{eff}= 50.8 µm σ b_{eff}= 34.6 µm <t >= 14’00’’
Level 4	N / Ne= 747.6 / 50 c_I = 32.2 % $\langle l_{eff} \rangle$= 269.7 µm $\langle b_{eff} \rangle$= 181.1 µm σ l_{eff}= 104.0 µm σ b_{eff}= 51.17 µm <t> = 0 ’’	N / Ne= 137.8 / 45 c_I = 2.7 % $\langle l_{eff} \rangle$= 212.75 µm $\langle b_{eff} \rangle$= 144.45 µm σ l_{eff}= 53.2 µm σ b_{eff}=39.4 µm <t >= 3’37’’	N / Ne = 3 / 3 c_I = 1.3 % $\langle l_{eff} \rangle$= 262.7 µm $\langle b_{eff} \rangle$= 142.1 µm σ l_{eff}= 89.3 µm σ b_{eff}= 30.1 µm <t>= 9’07’’	N / Ne = 0 / 0 c_I = 0 % $\langle l_{eff} \rangle$= 0 µm $\langle b_{eff} \rangle$= 0 µm σ l_{eff}= 0 µm σ b_{eff}= 0 µm <t> = 13’00’’

Table 1: Statistical data extracted from microscopic photographs for 4x4 time/space locations. Level 1 indicates the highest position for the removal of samples and level 4 the lowest in the tank (see Ref. [5]). The quantities are described in the nomenclature.

because smaller particles have smaller rising velocities (see chapter 5 and 7), the higher the time which passes before a sample is sucked out of the tank, the smaller the characteristic particle diameters are, which are determined by microscopic observations.

In Fig. 2 the results previously published in FIG. 5b of Ref. [5] are presented with some small improvements based on the additional statistical information obtained for 3.5, 11 and 13 minutes. Because each evaluation is based on five photographs, which were taken one after the other in a fast procedure, in table 1 also the mean time <t> of the observation is listed.

Differences between the first evaluation, published in Ref. [5], and this new one are in every case smaller than two percent in the ice concentration, except for the top level (level 1). In this single case for a longer time than 10’15’’ the correction is of the order of seven percent of the local ice concentration.

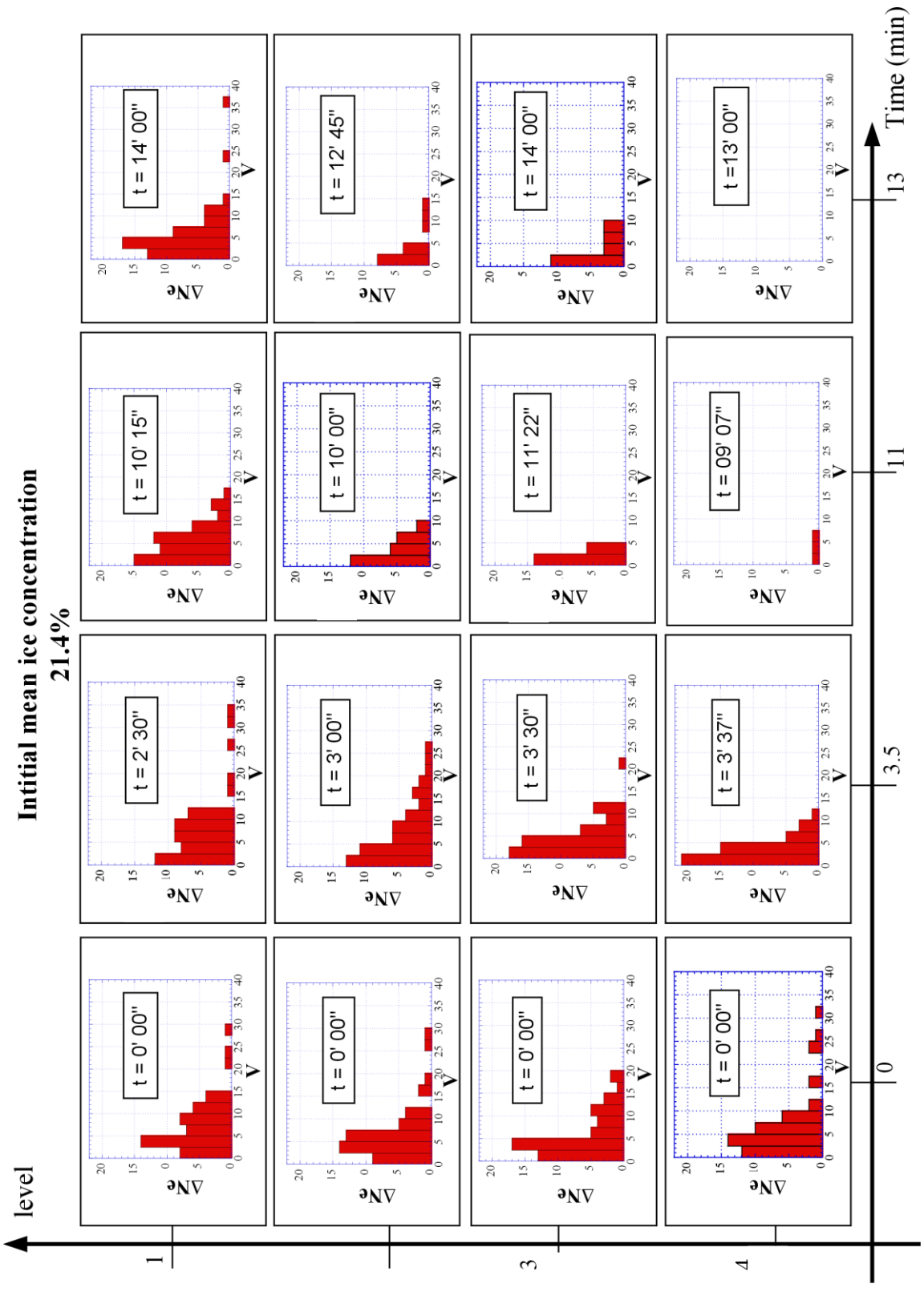

Figure 1: Histograms of the ice particles. Number of particles as a function of volume ($(10^6$ μm^3). The arrangement of the diagrams follows a time and spatial order, which is identical to the one in FIG. 7 of Ref. [5].

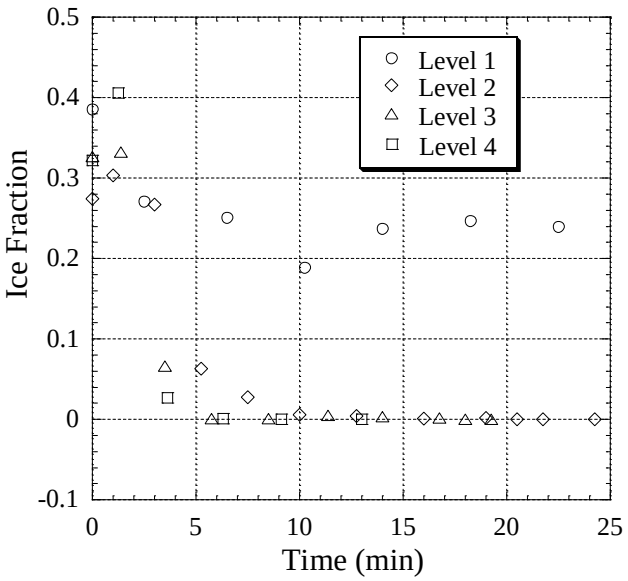

Figure 2: The ice fractions in the storage tank as a function of time are shown. These data have a higher accuracy compared to the results published in Ref. [5]. In the previous evaluations the particle sizes were only determined at time zero. Because the characteristic lengths and widths decrease as a function of time this leads to small corrections. As a result the ice concentrations, which are presented here, are somewhat smaller.

5. SETTLING VELOCITY OF ELLIPSOIDAL PARTICLES

Details on the derivation of the hindered settling velocity for spherical ice particles are presented in Ref. [6]. The main result is of twofold structure

$$v = \begin{cases} \dfrac{g d_p^2}{18\eta(\vartheta, c_I)} \left[\rho(\vartheta, c_I) - \rho(\vartheta, 1)\right], & c_I < c_{I_{\max}} \\ 0, & c_I = c_{I_{\max}}. \end{cases} \tag{12a,b}$$

In most of the calculations the quantity c_I in equation (12a) was set equal to 0. But this is not the case in the upper bound of the ice concentration. This result is valid for Reynolds numbers

$$\mathrm{Re} = \frac{v_I d_p \rho}{\eta} < 1, \tag{13}$$

and a drag coefficient of

$$C_D = \frac{24}{\mathrm{Re}}. \tag{14}$$

This formula can easily be derived. An estimation shows that in our case a characteristic Reynolds number is of the order 10^{-3}. Therefore, the observed and calculated phenomena are

clearly in the Stokes regime. In [10] generalized drag coefficient curves are published, which show slightly higher values for spheroidal particles with a shape factor

$$s = \frac{a}{\sqrt{cb}},$$

where a,b,c define the length of the half axis of the ellipsoids. For s=1 equation (14) applies.

6. BUOYANCY FORCE RELATED TO FLUID OR MIXTURE ?

In equation (12) the density of the ice slurry is taken as a reference to calculate the buoyancy forces. The following calculations were performed for two densities, the density of the ice slurry and of the water/additive (e.g. see FIG. 3). The second calculation procedure leads to smaller front propagation times, because the density difference is higher. Therefore, it is in beter agreement with our experimental observations. Because of that reason, numerical simulation results with the density of water/additive in the buoyancy force are presented in this article. But the correctness of the chosen method is not so clear to us and yields some material for further considerations. At least the chosen procedure corresponds with the technique, which is applied by many authors.

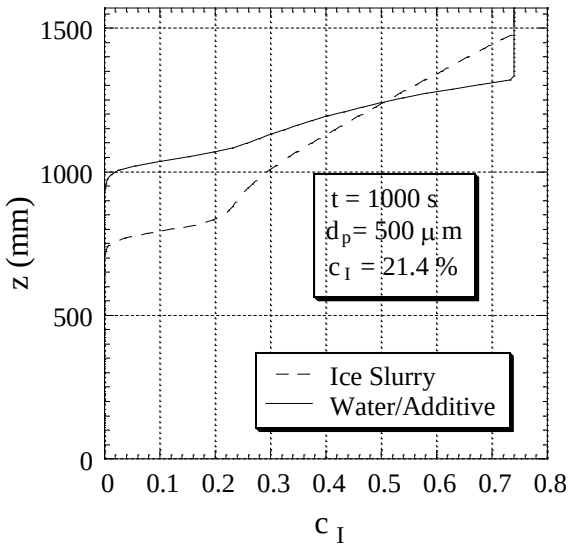

Figure 3: Two numerical calculations of an ice particle stratification with different reference densities in the buoyancy term. If the buoyancy - in a macroscopic view - is influenced by the overall density of the ice slurry, the buoyancy force is smaller and the front propagation time is larger. On the other hand the density of the water/additive leads to smaller propagation times and to a better agreement between experimental and numerical results. All the parameters of the numerical simulations are listed in Table 2.

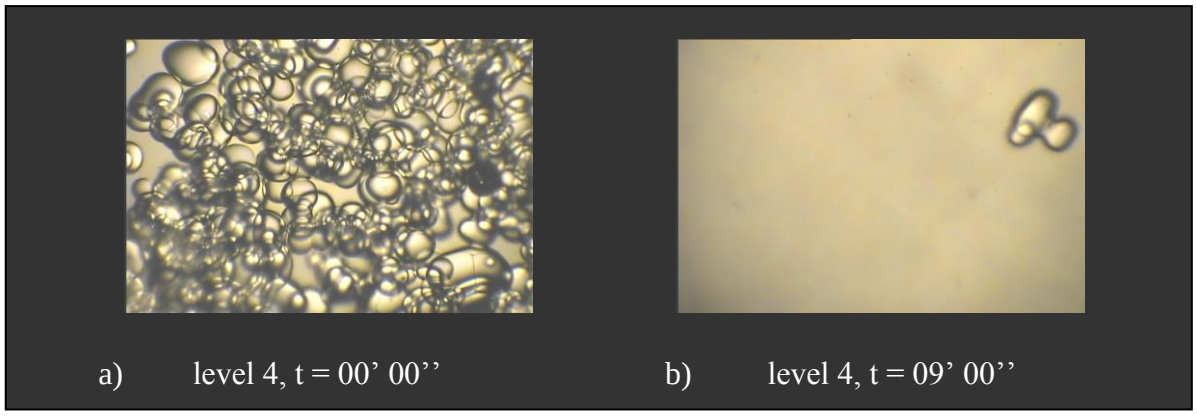

Figure 4: Two photographs (2384 μm*1603 μm) taken at different times at the fourth level (lowest position). Photo a) shows a domain full of ice particles and b) a cluster of three connected particles in a water/additive surrounding.

7. FURTHER NUMERICAL RESULTS OF ISOTHERMAL STRATIFICATION

In the following several results obtained by numerical simulations are presented. The main parameters for the calculations are given in Table 2. These results were worked out for two different ice concentrations, which were the basis for two classes of experiments. The two ice concentrations correspond to those in industrial applications.

Physical quantity	Symbol	Numerical value	Dimension
Time	t	0-3500	s
Height	h	1570	mm
Initial ice concentration	c_0	10.3 / 21.4	mass-%
Maximal ice concentration	c_{max}	74	mass-%
Number of time intervals	n	10 000	-
Number of space intervals	k	100	-
Diffusion coefficient (see Ref. [7])	D	0.00002	m^2/s
Initial talin concentration	c_A	10	mass-%
Temperature	ϑ	- 4.50 / - 5.45	°C
Particle diameter	d_p	100-750	μm

Table 2 : The parameters for the numerical simulations are listed.

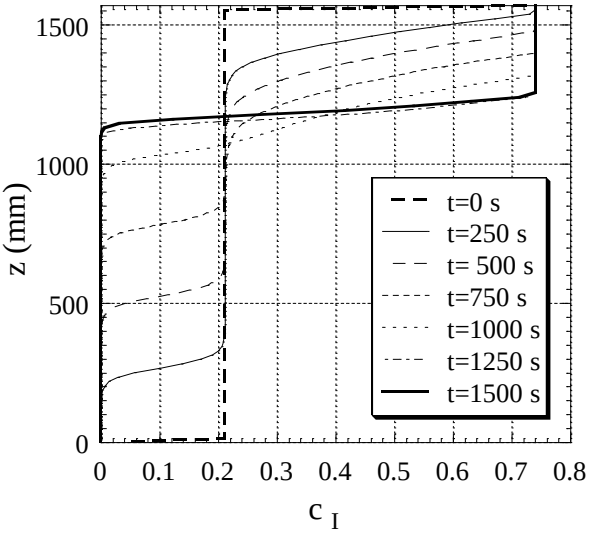

Figure 5: Ice particle stratification process with isothermal conditions. In this case the ice particle diameter was chosen to be 500 μm. The initial ice concentration of 21.4 % can be seen as a vertical line, indicating that the ice concentration is constant from the bottom (z=0) to the top of the tank (z=1570 mm). The profiles converge toward a steady state solution, which is obtained at circa 1500 s. At the beginning of the process the stratification is approximately linear in time.

Figure 6: In this figure the influence of the ice particle diameter on the stratification process is shown. The process was calculated to occur during 750 s. Five different diameters of spherical ice particles have been chosen. The velocity is proportional to the square of the diameter (see equation (12)). The steady state solution occurs much earlier, if the particles are larger. The curve corresponding to a particle diameter of 500 μm can also be found in FIG. 5.

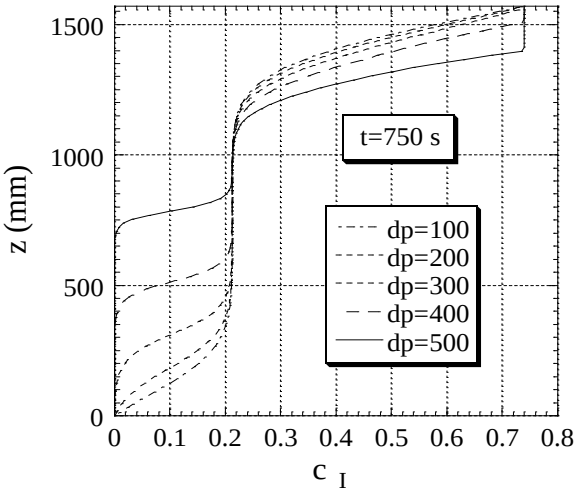

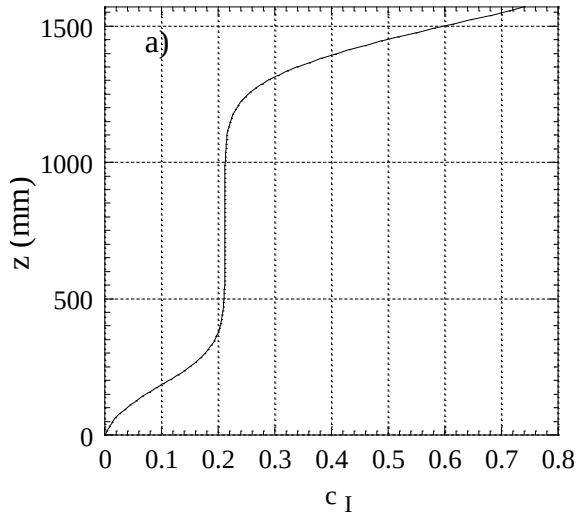

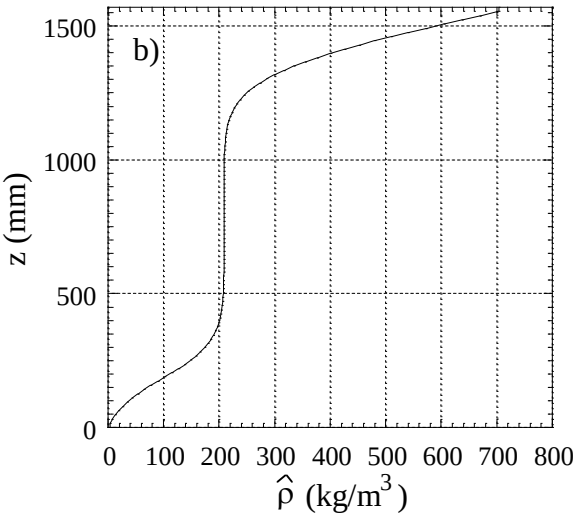

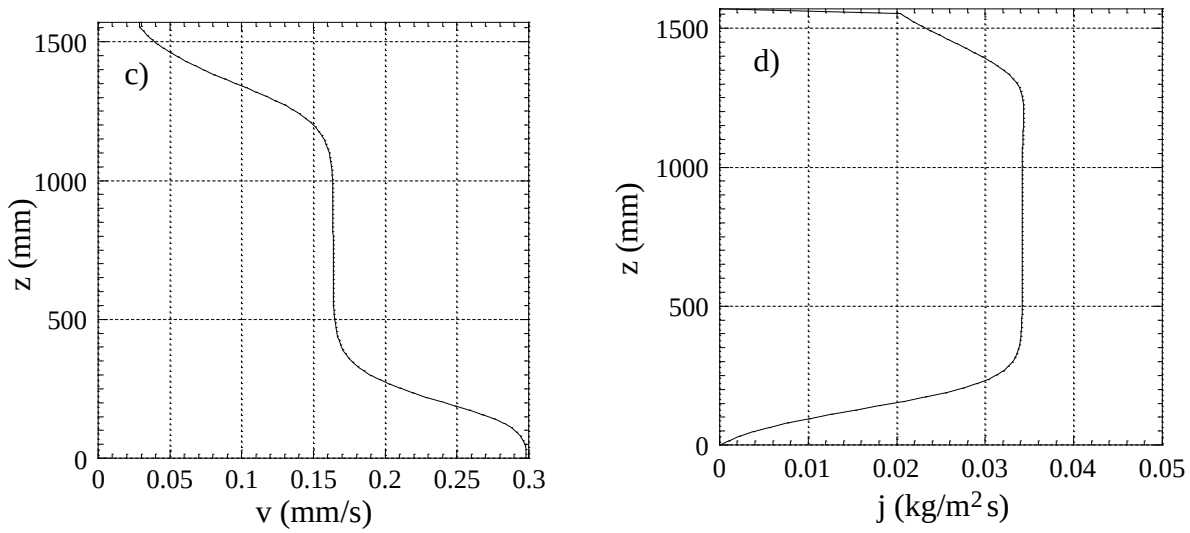

Figure 7: The ice concentration (a), the density component (b), the velocity (c), and the flux density (d) are shown for an ice particle diameter of 200 μm. The figure for the ice concentration can also be found in FIG. 6 with the parameter d_p=200 μm.

In FIG. 5 a stratification process as a function of time is shown. It reaches a steady-state solution after approximately 1500 s. The dependence on ice particle diameter is shown in FIG. 6. In FIG. 7 the most important physical quantities are presented. At the initial time (t=0) the ice particle field was assumed to be homogeneous. After this initial time the stratification process started to occur. A period of 750 s later the physical quantities have developed toward the distributions presented in the four graphs of FIG. 7.

8. FRONT PROPAGATION TIMES

Vuarnoz et al. have experimentally observed front propagation times in a storage tank for two initial ice concentrations [5] (see FIG. 8). With the same experimental device the ice particle statistics was determined. Studying Table 1 we can state that the particles are approximately ellipsoidal with a mean width to mean length ratio of 0.7. If we assume that we would have spherical particles with identical volume the equivalent diameter would be approximately d_p=200 μm. With this parameter the numerical simulations cannot explain the observed front propagation times, which are the times when the last particles are observed at a level of observation. The only uncertain quantities in the simulations are the particle diameter and the viscosity, because of the time behaviour. The viscosity was calculated with formula (5.2/5a) in Ref. [6]. The formula corresponds quite well to the Thomas model. Then we assumed that only the particle diameter is a free parameter and determined the optimal values to describe the measurements. The results are consistent in the sense that for 10.3 % and 21.4 % initial ice concentrations, in both cases, the obtained diameters are circa 500 μm. For the smaller initial ice concentration the values are a little higher, with an upper bound of 750 μm.

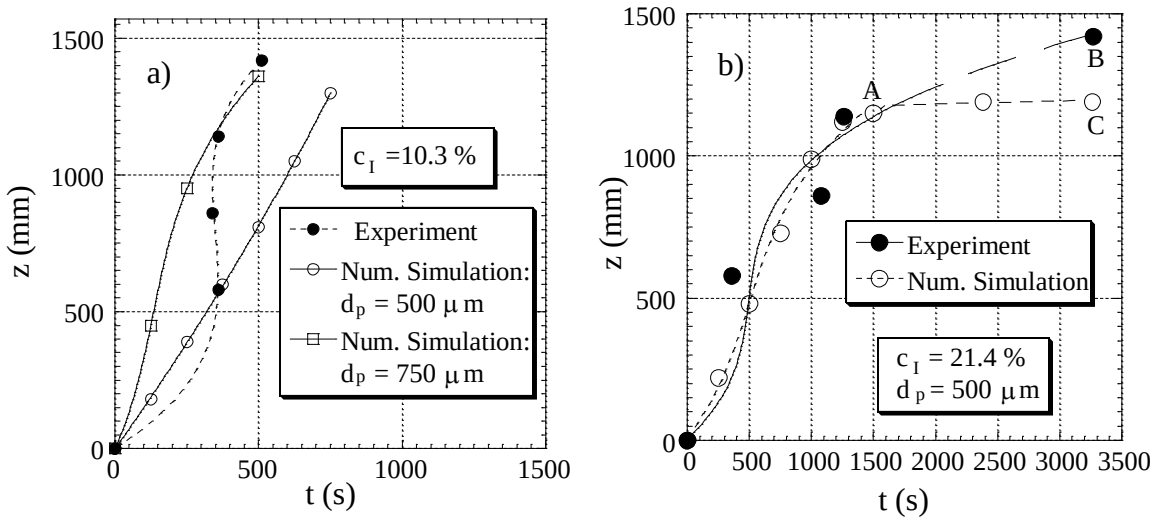

Figure 8: Experimental and theoretical results of ice particle front propagations. The three equal times in the experimental data in figure a) are explained by the fact that in the measurements of the front propagation time for each level the experiment was repeated. In the second figure b) the experimental results reach a higher level (A-B), because an ice layer is lifted out of the fluid. This phenomenon is not described by the physical model (A-C).

The experimental observations can only be explained, if we assume that a small number of ice particles stick together. And this is indeed observed in most of our photographs, e.g. see in Ref. [5] and FIG. 9.

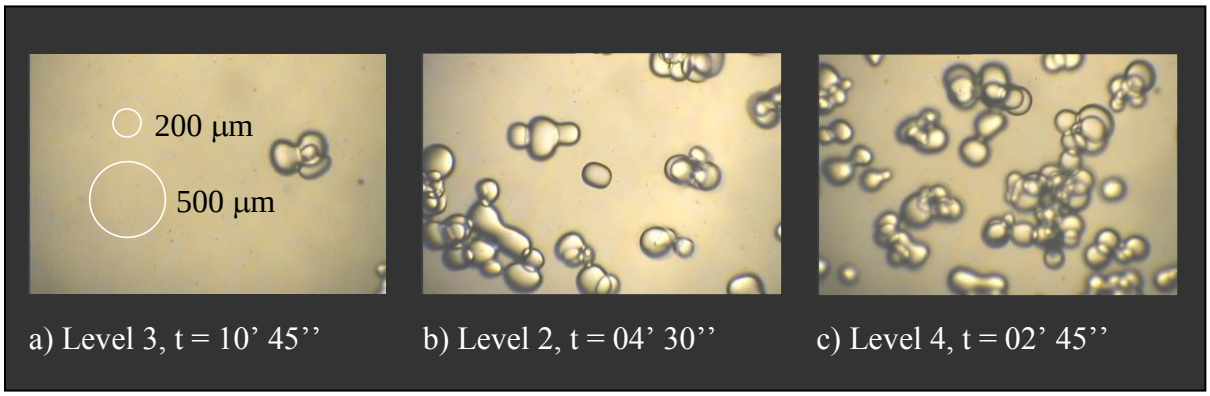

Figure 9: Three photographs (2384 μm*1603 μm) taken at different times and positions. They clearly show some small ice particle clusters. For comparison in figure a) on the left two circles of diameter 200 μm and 500 μm are shown. In figure b) in the left lower corner a particle is seen which originally consisted of two particles. Even the boundary between these two particles has vanished. Agglomeration and combination of such a type may explain the observed time behaviour. In c) also meso-scale clusters are observed.

Front propagation times were determined from figures as FIG. 5. The z values on the ordinate (on the left) determine the front propagation times. The diffusion "tails" were not taken into consideration.

Clusters show higher drag coefficients than spheres. Therefore, the actual cluster sizes will be even a little larger than 500 μm. The higher buoyancy forces of larger particles is compensated by the larger drag force caused by the irregular shapes of the clusters.

9. CONCLUSIONS AND OUTLOOK

The numerical simulation results are in good agreement with experimentally observed front propagation times. But the agreement is only obtained by assuming too large ice particle diameters in the numerical simulations. This observation can be explained by assuming a development of a large number of medium-sized clusters in the suspension. And such clusters are really observed. Some are shown in photographs taken of samples of ice slurries with different ice concentrations.

Some uncertainity in the choice of the density in the description of the buoyancy force in Stokes law must be clarified and the studies of clusters should be further improved. Further statistical material on clusters (mean equivalent diameters, mean drag coefficients, etc.) would be very useful informations to continue and improve the work in this important domain of ice slurry research.

NOMENCLATURE

Standard

c_p	specific heat at constant pressure
c	concentration, fraction
d	diameter
div	divergence operator
D	diffusion “constant”, resp. function
div	divergence operator
h	height
$\vec{j}$	flux density
k	number of space increments
k	thermal conductivity
l	length
ℓ	latent heat
n	number of time intervals
N	Number of particles
q_p	source and sink
$\dot{q}$	heat flux density
t	time
T	absolute temperature
U	overall heat transfer coefficient
v	velocity component in axial direction
$\vec{v}$	vector of velocity

V volume
w width
W work (heat) to melt a single ice particle

Greek

α thermal diffusivity
χ general variable
Δ Laplace operator
$\vec{\gamma}$ normal boundary vector
Γ domain of ice slurry in a storage vessel
$\delta\Gamma$ boundary of fluid domain
η dynamic viscosity
ϑ temperature
T temperature
ρ density
$\hat{\rho}$ density of ice (particle) component
σ standard deviation
∇ gradient operator

Indices

A ambient
e evaluated
eff effective
I ice
p particle (ice particle)

ACKNOWLEDGEMENTS

The "*Gebert Rüf Stiftung*" and the „*Haute École Suisse Occidentale (Hes-so)*" are kindly acknowledged for funding our applied research.

REFERENCES

[1] Y. Kozawa, M. Tanino, *Ice-water two-phase flow behavior in ice heat storage systems.* First Workshop on Ice Slurries of the International Institute of Refrigeration IIF/IIR, 147-157, Yverdon-les-Bains, Switzerland, 27-28 May (1999).

[2] Y. Kozawa, N. Aizawa, M. Tanino, *Study on ice storing characteristics in dynamic-type ice storage system by using supercooled water.* Third Workshop on Ice Slurries of the International Institute of Refrigeration IIF/ IIR, 87-96, Lucerne, Switzerland, 16-18 May (2001).

[3] R. Hong, M. Kawaji, V. Goldstein, *Numerical investigation of ice slurry flow and heat transfer in a scraped ice generator and a storage tank.* Third Workshop on Ice Slurries

of the International Institute of Refrigeration IIF/IIR, 119-125, Lucerne, Switzerland, 16-18 May (2001).

[4] F. Meili, O. Sari, D. Vuarnoz, P. W. Egolf, *Storage and mixing of ice slurries in tanks*. Third Workshop on Ice Slurries of the International Institute of Refrigeration IIF/IIR, 97-104, Lucerne, Switzerland, 16-18 May (2001).

[5] D. Vuarnoz, O. Sari, P. W. Egolf, *Correlations between temperature and particle distributions of ice slurry in a storage tank*. Fourth Workshop on Ice Slurries of the International Institute of Refrigeration IIF/ IIR, 123-134, Osaka, Japan (2001).

[6] P. W. Egolf, D. Vuarnoz, O. Sari, *A model to calculate dynamical and steady-state behaviour of ice particles in ice slurry storage tanks*. Fourth Workshop on Ice Slurries of the International Institute of Refrigeration IIF/IIR, 25-39, Osaka, Japan (2001).

[7] P. W. Egolf, D. Vuarnoz, O. Sari, *Particle Fields of Ice Slurries with Stratifications and Melting.* International Conference on Solid-Liquid Phase Change' 02. Part of the project: Fundamental Research on Thermal Energy Storage to Preserve Environment, 99-104, Tokyo, 10-11 January, 2002.

[8] Egolf P. W., Manz H. Theory and modeling of phase change materials with and without mushy regions. *Int. J. Heat Mass Transfer*, **37** (18), 2917-2924 (1994).

[9] P. W. Egolf, B. Frei, *Continuous-properties model for melting and freezing applied to fine-crystalline ice slurries*, First Workshop on Ice Slurries of the International Institute of Refrigeration IIF/IIR, 25-40, Yverdon-les-Bains, Switzerland, 27-28 May (1999).

[10] E. J. Wasp, J. P. Kenny, R.L. Gandhi, *Solid-liquid flow slurry pipeline transportation*. Series on Bulk Materials Handling Vol. 1, No. 4 (1977).